Fluorescent Probes Hot Paper

International Edition: DOI: 10.1002/anie.201500941
German Edition: DOI: 10.1002/ange.201500941

Strained Cyclooctyne as a Molecular Platform for Construction of Multimodal Imaging Probes**

Yao Sun, Xiaowei Ma, Kai Cheng, Biying Wu, Jianli Duan, Hao Chen, Lihong Bu, Ruiping Zhang, Xianming Hu, Zixin Deng, Lei Xing, Xuechuan Hong, and Zhen Cheng**

Abstract: *Small-molecule-based multimodal and multifunctional imaging probes play prominent roles in biomedical research and have high clinical translation ability. A novel multimodal imaging platform using base-catalyzed double addition of thiols to a strained internal alkyne such as bicyclo[6.1.0]nonyne has been established in this study, thus allowing highly selective assembly of various functional units in a protecting-group-free manner. Using this molecular platform, novel dual-modality (PET and NIRF) uPAR-targeted imaging probe: ^{64}Cu-CHS1 was prepared and evaluated in U87MG cells and tumor-bearing mice models. The excellent PET/NIRF imaging characteristics such as good tumor uptake (3.69 %ID/g at 2 h post-injection), high tumor contrast, and specificity were achieved in the small-animal models. These attractive imaging properties make ^{64}Cu-CHS1 a promising probe for clinical use.*

Multimodality and multifunctional imaging has evolved into a fast-growing research field with goals of detecting and measuring biological processes in vivo non-invasively.[1] Up to now, a variety of chemical platforms such as small molecules,[2] proteins,[3] polymers,[4] and nanomaterials[5] have been actively explored to construct multimodal and multifunctional imaging probes, and these platforms own different advantages and disadvantages.[6] Of all these platforms, small-molecule-based imaging probes remain desirable candidates for clinical applications. However, multiple synthetic steps and extensive use of protection-deprotection strategies are required for the preparation of these probes using reported approaches.[2a,b] Moreover, they also suffer from the difficulty of obtaining pure and single species because of the issues of regio- and diastereoselectivity.[7] Therefore, developing effective small-molecule platforms with facile chemical methods for construction of multifunctional imaging probes with high flexibility, efficiency, chemoselectivity, and clinical translation ability are still highly demanded.

Alkyne–azide click chemistry represents an important class of chemical reactions for convenient preparation of many novel chemical entities, and plays important roles in drug discovery, chemical biology, and molecular imaging.[8] For instance, the strain-promoted alkyne–azide cycloaddition (SPAAC) chemistry has been highlighted to assemble monofunctional imaging probes for profiling glycans on living cells.[9] These strained cyclooctynes display not only good biocompatibilty and low cytotoxicity, but also higher reactivity than general cycloalkynes.[9] Therefore they have been widely used for new bioorthogonal reactions besides SPAAC.[10] However, only one molecule is coupled and multiple functional molecules cannot be directly assembled. Recently, thiol–yne click chemistry has been shown to be a highly efficient reaction between thiols and alkynes.[11] Although two thiolated units could be added across a terminal linear alkyne sequentially by photoinduction, it could produce some unavoidable by-products (disulfides) and also cause problems in assembling light-sensitive molecules (optical probes).[11] The failure to consecutively add two thiols into an cycloalkyne has been reported,[12] thus suggesting that it is still a challenging substrate for photoclick chemistry and prompts us to explore new chemistry to efficiently incorporate various functional units into strained cyclooctyne scaffolds for the construction of multimodality probes (Scheme 1 a).

A powerful synergy can be achieved by a multilabel-tumor-targeted probe combining positron emission tomography (PET) imaging for localization of a tumor in the whole body, and near-infrared fluorescence (NIRF) imaging for subsequent accurate delineation of tumor lesions and resection margins. Numerous studies have implicated that the urokinase-type plasminogen activator (uPA) and its receptor (uPAR) are of special importance in cancer invasion, and uPAR has been considered as an attractive target for both cancer imaging and therapy.[13] AE105 is a small linear peptide with high binding affinity to uPAR.[14] Targeting uPAR with

[*] Y. Sun, B. Y. Wu, J. L. Duan, H. Chen, Prof. X. M. Hu, Z. X. Deng, X. C. Hong
State Key Laboratory of Virology, Key Laboratory of Combinatorial Biosynthesis and Drug Discovery, Ministry of Education, and Wuhan University School of Pharmaceutical Sciences
Wuhan 430071 (China)
E-mail: xhy78@whu.edu.cn

Y. Sun, Dr. X. W. Ma, K. Cheng, H. Chen, L. H. Bu, R. P. Zhang, L. Xing, Prof. Z. Cheng
Molecular Imaging Program at Stanford (MIPS), Bio-X Program, and Department of Radiology, Stanford University
California, 94305-5344 (USA)
E-mail: zcheng@stanford.edu

[**] This work was partially supported by the Office of Science (BER), U.S. Department of Energy (DE-SC0008397), NIH In vivo Cellular Molecular Imaging Center (ICMIC) grant P50 CA114747, NSFC (81373254, 81301268 and 21390402), NSFHP (2014CFB704), International S&T Cooperation Program of China (2015DFA30440, 2014DFB30020), Key Project of Chinese Ministry of Education (313040), Academic Award for Excellent Ph.D. Candidates Founded by Ministry of Education of China (5052012306001), China Scholarship Council Fellowship, and the Fundamental Research Funds for the Central Universities.

Supporting information for this article is available on the WWW under http://dx.doi.org/10.1002/anie.201500941.

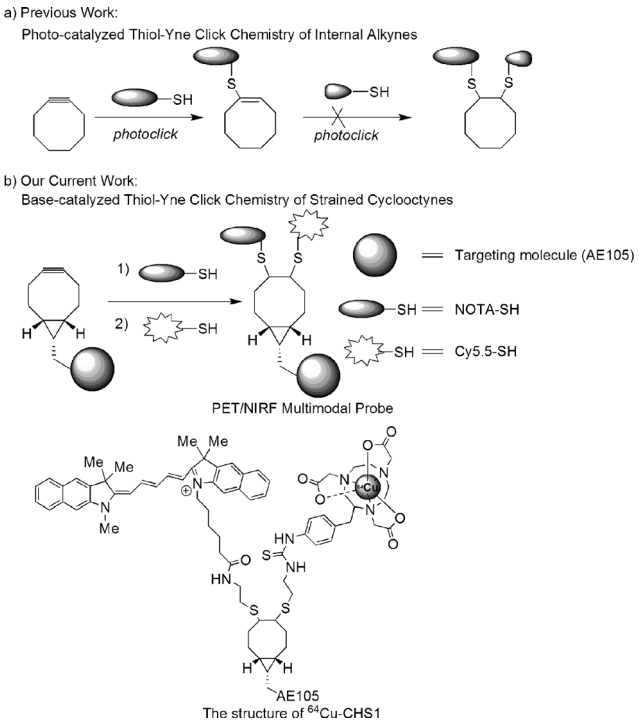

Scheme 1. A new strategy for the construction of multimodal imaging probes. a) The photocatalyzed thiol–yne reaction. b) Approach discussed in the present work.

multivalent or multimodality AE105-based imaging probes in vivo have not been reported yet.

In this study, for a proof of concept, the PET and optical imaging dual-modality probe ^{64}Cu-CHS1 (Scheme 1b) was concisely prepared where the optical reporter Cy5.5 for NIRF imaging and ^{64}Cu-1,4,7-triazacyclononane-triacetic acid (NOTA) for PET are successfully integrated, and the AE105 is coupled with the strained bicyclo[6.1.0]nonyne (BCN) through an amide bond. The targeting ability and PET/NIRF imaging properties of ^{64}Cu-CHS1 have been demonstrated on U87 MG tumor mice models, thus highlighting the promising clinical translation potential of the probe.

Our initial study began with the introduction of simple functional molecules: 3-mercaptoacetic acid (**2**; 3-MPA) into the L-Phe modified BCN **1** scaffold for optimization studies (Table 1). A range of organic bases were screened for the thiol addition reaction in DMSO/H_2O (1:1). The data reveal that the ratio of monoadduct **1a** and double-adduct **1b** can be controlled by adding different equivalents of the thiols and catalysts (Table 1). Strained cyclooctyne can undergo the cycloaddition reactions spontaneously in the absence of amines in 25–37% yields (entries 1 and 5).[15] However, the yields of **1a** were increased to 55–67% when the amine bases DIPEA, NEt_3, and DBU (0.15 equiv) were used (entries 2–4). Furthermore, **1b** was favored when 4.0 equivalents of thiols were used. Only **1b** was obtained in the case of DBU (entry 8). It was also observed that in the presence of the radical scavenger TEMPO (2 equiv) the yield of the adducts was significantly reduced, thus suggesting a possible radical-based mechanism. The structures of **1a** and **1b** were confirmed by ESI-MS, and ^{1}H NMR and ^{13}C NMR spectroscopy (see Figures S1 and S2 in the Supporting Information). Dibenzocyclooctyne-amine (DIBAC) was further evaluated as a potential multifunctional scaffold to incorporate two 2-aminoethanethiols (2-AET) in the presence of DBU, and the monoadduct was obtained in high yield as the sole product (see Scheme S1 and Figure S3 in the Supporting Information).

Table 1: Base-catalyzed thiol–cyclooctyne chemistry.[a]

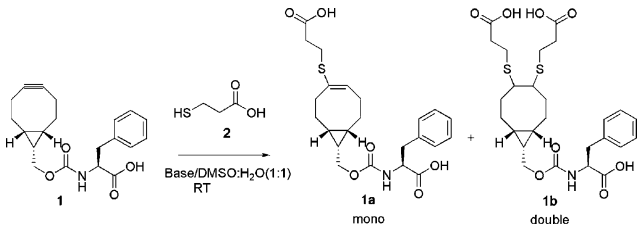

Entry	Catalyst	t [h]	Thiol (equiv)	Yield [%][b]	**1a/1b**
1	–	4	1.0	25	100:0
2	NEt_3	4	1.0	55	90:10
3	DIPEA	4	1.0	67	92:8
4	DBU	4	1.0	61	80:20
5	–	4	4.0	37	40:60
6	NEt_3	4	4.0	57	17:83
7	DIPEA	4	4.0	65	12:88
8	DBU	4	4.0	70	0:100

[a] Reaction conditions: [cyclooctyne] = 0.20 M in DMSO/H_2O (1:1), catalyst = 0.15 equiv. [b] Yield of the isolated product (major) and calculated based on the starting alkyne.

Based on the above results, we then explored assembly of more complex biomolecules on the BCN scaffold. Firstly, a series of scaffold molecules [c(RGDfK)-BCN (**3a**), AE105-BCN (**3b**), c(RGDyK)-BCN (**3c**), and DOTA-BCN (**3d**)] and functional thiols [2-AET-NOTA (**Y1**), 2-AET-Cy5.5 (**Y2**), 3-MPA-c(RGDfK) (**X1**), and 3-MPA-AE105 (**X2**)] were prepared by traditional coupling chemistry (see the Supporting Information). As shown in Table 2, various multifunctional molecules were successfully prepared. The yields were increased as the steric hindrance of the thiols decreased (entries 1–3). Furthermore, monovalent uPAR-targeted PET and NIRF probes were successfully prepared by incorporation of NOTA (**Y1**) or Cy5.5 motifs (**Y2**) in 43 and 26% yields, respectively (entries 4 and 5). Treatment of c(RGDyK)-BCN with 3-MPA (4 equiv) resulted in the formation of the double-adduct **6a** in 58% yield (entry 6), and it was fully characterized by ESI-MS and ^{1}HNMR analyses (see Figure S4 in the Supporting Information). However, no double-addition product was obtained when two c(RGDfC) molecules were applied in the coupling (entry 7). We hypothesized that the bulky macrocycles of c(RGDfC) might prevent the second thiol addition. To minimize the steric hindrance, 3-MPA-c(RGDfK) was introduced into the cycloaddition system instead of c(RGDfC). To our delight, the desired trimer RGD (**6c**) and dimer RGD (**6d**) compounds were successfully prepared (entries 8 and 9). The mono-RGD-based **4a** (DOTA-BCN-RGDfK) was used

Table 2: Base-catalyzed addition of various functional molecules into BCN-based scaffolds.

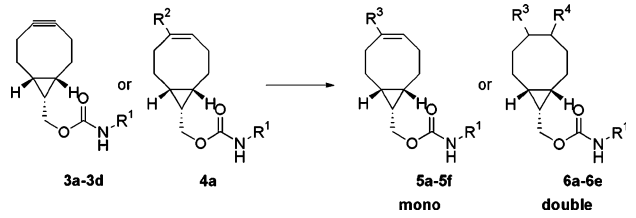

Entry[a]	BCN scaffold	t [h]	Product	Yield [%]
1	R^1 = RGDfK (**3a**)	12	R^3 = RGDfC (**5a**)	30
2	R^1 = RGDfK (**3a**)	12	R^3 = 3-MPA-RGDfC (**5b**)	38
3	R^1 = RGDfK (**3a**)	6	R^3 = 2-AET-NOTA (**5c**)	45
4	R^1 = AE105 (**3b**)	6	R^3 = 2-AET-NOTA (**5d**)	43
5	R^1 = AE105 (**3b**)	6	R^3 = 2-AET-Cy5.5 (**5e**)	26
6	R^1 = RGDyK (**3c**)	6	R^3 = R^4 = 3-MPA (**6a**)	58
7	R^1 = RGDyK (**3c**)	24	R^3 = R^4 = RGDfC (**6b**)	0[b]
8	R^1 = RGDyK (**3c**)	18	R^3 = R^4 = 3-MPA-RGDfK (**6c**)	23
9	R^1 = DOTA (**3d**)	18	R^3 = R^4 = 3-MPA-RGDfK (**6d**)	25
10	R^1 = DOTA R^2 = RGDfK (**4a**)	12	R^3 = 3-MPA-AE105 (**6e**)	17

[a] Catalyst: DIPEA for entries 1–5; DBU for entries 6–10. [b] The MS data indicate that product is the monoadduct.

as a substrate to incorporate the AE105 unit for construction the heterodimer-peptide-based probe precursor **6e** in 17% yield (entry 10). Finally, the uPAR-targeted PET/NIRF probe CHS1 was successfully prepared (see Scheme S2 in the Supporting Information). The CHS1 probe was purified by HPLC and characterized by MALDI-TOF [Calcd. for $C_{145}H_{194}N_{25}O_{26}S_3^+$ ($[M+H]^+$): 2797.4, found: m/z 2798.1 (see Figure S5 in the Supporting Information)]. The absorbance and fluorescence emission spectra indicated that CHS1 maintained the optical properties with an emission maximum at $\lambda = 700$ nm in a PBS buffer (see Figure S6 in the Supporting Information).

Compared with other small-molecule scaffolds, this BCN mainly has the following advantages. First, the thiol–yne reaction can be effectively catalyzed by simple and cheap organic bases (DIPEA or DBU) under mild reaction conditions (ambient temperature and aqueous medium), and can tolerate a wide range of functional groups such as NH_2, CO_2H, and OH (Table 1 and 2). Secondly, the synthesis of BCN-based multimodality probes is simple and straightforward. It is a concise and protecting-group-free synthetic route, and the formation of monoaddition or double-addition adducts can be controlled (Table 1).

To demonstrate the cell-uptake and receptor specificity of CHS1, U87 MG cells were selected to evaluate the targeting ability and specificity of CHS1 because of their high uPAR expression.[16] As shown in Figure S7A (see the Supporting Information), a strong fluorescent signal was observed on cell membranes after 30 minutes of incubation with CHS1 (10 nM). Weak fluorescence of U87MG cells was observed in the presence of the blocking agent AE105 (1 μM), thus suggesting the specific cellular uptake of CHS1 in vitro. CHS1 was efficiently labelled with ^{64}Cu at ambient temperature within 30 minutes and was purified by RP-HPLC in high yield and purity (>95%; see Figure S8A in the Supporting Information). The specific activity of ^{64}Cu-CHS1 was about 800 mCi μmol^{-1}. ^{64}Cu-CHS1 displayed excellent stability in mouse serum and showed no release of ^{64}Cu over a period of 12 hours (see Figure S8B). As anticipated, ^{64}Cu-CHS1 exhibited good uptake in U87MG cells (see Figure S7B). In the blocking group, the uptake was significantly reduced, thus indicating the target specificity of ^{64}Cu-CHS1. Thus, ^{64}Cu-CHS1 was easily and reliably produced and exhibited high stability for in vivo applications.

The U87MG-tumor-bearing nude mice ($n = 4$) were injected with 100 μCi (1 nmol) of ^{64}Cu-CHS1 and were imaged with IVIS and micro-PET/CT separately. From both NIRF and PET imaging, the U87MG tumor could be clearly visualized from the surrounding background tissue, even at 1 h p.i., with good tumor contrasts for all-time points investigated (Figure 1A and B). The specificity of ^{64}Cu-

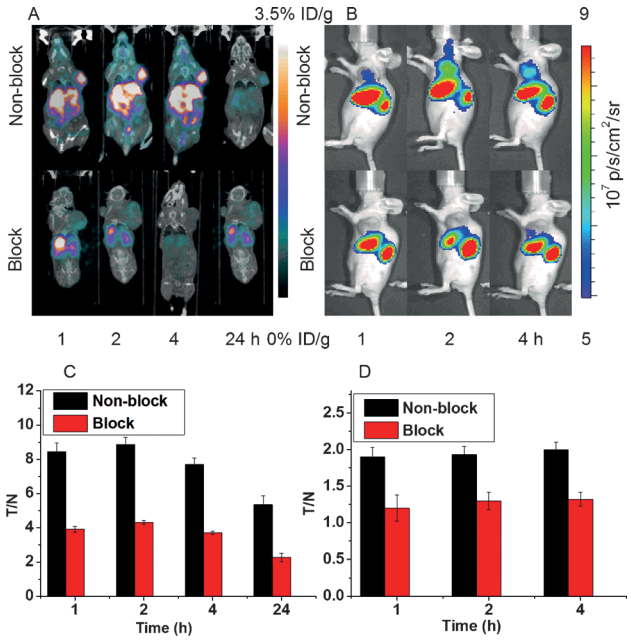

Figure 1. A) The PET/CT images of U87MG-tumor-bearing mice (red rings indicate the location of the tumor, $n = 4$ per group) acquired at 1, 2, 4, and 24 h after tail vein injection of ^{64}Cu-CHS1 with and without the blocking agent AE105. B) The fluorescence images of U87MG tumors at 1, 2, and 4 h after tail vein injection of ^{64}Cu-CHS1 with and without the blocking agent AE105. C) PET imaging, represented as the tumor-to-normal tissue (T/N) ratio for ^{64}Cu-CHS1 at 1, 2, 4, and 24 h. D) NIRF imaging, represented as (T/N) ratio for the ^{64}Cu-CHS1 probe (black bar) and blocking group (red bar) at 1, 2, and 4 h.

CHS1 for uPAR was confirmed by the blocking experiment, in which tumor signals were successfully reduced after co-injection of unlabeled AE105 with ^{64}Cu-CHS1 for both PET and NIRF imaging. Quantitative analysis of PET images further revealed that the tumor uptake values of ^{64}Cu-CHS1 were gradually increased from 1 to 2 hours and were reduced at 24 hours after injection, with (3.55 ± 0.30), (3.69 ± 0.21), (3.45 ± 0.20), and (0.91 ± 0.14)% ID/g at 1, 2, 4 and 24 hours, respectively (see Figure S9A in the Supporting Information).

Significantly lower tumor uptake for the blocking-dose group were observed, with the values of (0.42 ± 0.04), (0.43 ± 0.02), (0.45 ± 0.05), and (0.18 ± 0.02) % ID/g at 1, 2, 4 and 24 hours, respectively. The fluorescence intensities in the tumor and blocking group are depicted in Figure S9B. Compared with the normal group, lower fluorescence signals were observed at all-time points in the blocking group. The PET signal intensity ratios between the tumor and normal tissue (T/N) for ^{64}Cu-CHS1 are shown in Figure 1C. Obviously, the highest tumor contrast was obtained at the 2 hour time point for ^{64}Cu-CHS1, with a T/N value of (8.86 ± 0.43). The NIRF intensity ratios (T/N) for ^{64}Cu-CHS1 were shown in Figure 1D. At all-time points, the T/N ratios of normal group were significantly higher than those of the blocking group. Biodistribution studies were evaluated for ^{64}Cu-CHS1 in major organs. The tumor uptake value was (0.94 ± 0.12) % ID/g at 24 hours (see Figure S10 in the Supporting Information). In addition, a slightly higher accumulation was observed in the liver $(1.18 \pm 0.02$ % ID/g) and a similar level of accumulation was found in the kidney. The accumulation both in the liver and kidney suggests the clearance routes of ^{64}Cu-CHS1 through hepatobiliary and renal systems. Importantly, much lower tumor uptake was obtained [(0.16 ± 0.03) % ID/g] in the presence of the blocking agent, thus indicating the specific targeting properties of ^{64}Cu-CHS1 in vivo. The results of biodistribution also matched well with the PET and NIRF imaging data.

In summary, we have developed base-catalyzed thiol–yne chemistry for facile and controllable assembly of multifunctional molecules (targeting or reporting moieties). The small-molecule BCN scaffold has been identified as a new and promising imaging platform. Using this strained internal alkyne platform, uPAR-targeted imaging probes were successfully prepared. The PET/NIRF multimodality imaging probe ^{64}Cu-CHS1 has demonstrated excellent imaging characteristics in vivo and has high clinical and translational potential. It may find important applications in clinics for cancer diagnosis, image-guided surgery, and cancer patient management. The base-catalyzed thiol–yne chemistry and this type of BCN platform provide unprecedented opportunities for the construction of a variety of biologically interesting molecules and materials.

Keywords: alkynes · fluorescence · imaging agents · strained molecules · thiols

How to cite: *Angew. Chem. Int. Ed.* **2015**, *54*, 5981–5984
Angew. Chem. **2015**, *127*, 6079–6082

[1] a) L. Bu, X. Ma, Y. Tu, B. Shen, Z. Cheng, *Curr. Pharm. Biotechnol.* **2014**, *14*, 723–732; b) M. Rudin, R. Weissleder, *Nat. Rev. Drug Discovery* **2003**, *2*, 123–131; c) R. H. Kimura, Z. Miao, Z. Cheng, S. S. Gambhir, J. R. Cochran, *Bioconjugate Chem.* **2010**, *21*, 436–444.

[2] a) W. Liu, G. Y. Hao, M. Long, T. Anthony, J. T. Hsieh, X. K. Sun, *Angew. Chem. Int. Ed.* **2009**, *48*, 7346–7349; *Angew. Chem.* **2009**, *121*, 7482–7485; b) C. Q. Tu, R. Nagao, A. Y. Louie, *Angew. Chem. Int. Ed.* **2009**, *48*, 6547–6551; *Angew. Chem.* **2009**, *121*, 6669–6673.

[3] S. Hoppmann, Z. Miao, S. L. Liu, H. G. Liu, G. Ren, B. Ande, Z. Cheng, *Bioconjugate Chem.* **2011**, *22*, 413–421.

[4] a) L. Röglin, E. H. M. Lempens, E. W. Meijer, *Angew. Chem. Int. Ed.* **2011**, *50*, 102–112; *Angew. Chem.* **2011**, *123*, 106–117; b) Q. L. Fan, K. Cheng, X. Hu, X. W. Ma, R. P. Zhang, M. Yang, X. M. Lu, L. Xing, W. Huang, S. S. Gambhir, Z. Cheng, *J. Am. Chem. Soc.* **2014**, *136*, 15185–15194.

[5] a) L. Cheng, K. Yang, Y. G. Li, J. H. Chen, C. Wang, M. W. Shao, S. T. Lee, Z. Liu, *Angew. Chem. Int. Ed.* **2011**, *50*, 7385–7390; *Angew. Chem.* **2011**, *123*, 7523–7528; b) K. Cheng, S. Kothapalli, H. Liu, A. L. Koh, J. V. Jokerst, H. Jiang, M. Yang, J. Li, J. Levi, J. C. Wu, S. S. Gambhir, Z. Cheng, *J. Am. Chem. Soc.* **2014**, *136*, 3560–3571.

[6] A. Louie, *Chem. Rev.* **2010**, *110*, 3146–3195.

[7] a) X. F. Zhang, H. G. Liu, Z. Miao, R. Kimura, F. Y. Fan, Z. Cheng, *Bioorg. Med. Chem. Lett.* **2011**, *21*, 3423–3426; b) Y. H. Wang, Z. Miao, G. Ren, Y. D. Xu, Z. Cheng, *Chem. Commun.* **2014**, *50*, 12832–12835.

[8] a) V. V. Rostovtsev, L. G. Green, V. V. Fokin, K. B. Sharpless, *Angew. Chem. Int. Ed.* **2002**, *41*, 2596–2599; *Angew. Chem.* **2002**, *114*, 2708–2711; b) P. Thirumurugan, D. Matosiuk, K. Jozwiak, *Chem. Rev.* **2013**, *113*, 4905–4979; c) E. I. Sun, L. Josepbson, R. Weissleder, *Mol. Imaging* **2006**, *5*, 122–128.

[9] a) E. M. Sletten, C. R. Bertozzi, *Angew. Chem. Int. Ed.* **2009**, *48*, 6974–6998; *Angew. Chem.* **2009**, *121*, 7108–7133; b) D. M. Beal, L. H. Jones, *Angew. Chem. Int. Ed.* **2012**, *51*, 6320–6326; *Angew. Chem.* **2012**, *124*, 6426–6432.

[10] a) T. H. Poole, J. A. Reisz, W. L. Zhao, L. B. Poole, C. M. Furdui, S. B. King, *J. Am. Chem. Soc.* **2014**, *136*, 6167–6170; b) S. Wallace, J. W. Chin, *Chem. Sci.* **2014**, *5*, 1742–1744.

[11] a) R. Hoogenboom, *Angew. Chem. Int. Ed.* **2010**, *49*, 3415–3417; *Angew. Chem.* **2010**, *122*, 3489–3491; b) J. W. Chan, C. E. Hoyle, A. B. Lowe, *J. Am. Chem. Soc.* **2009**, *131*, 5751–5753; c) M. Minozzi, A. Monesi, D. Nanni, P. Spagnolo, N. Marchetti, A. Massi, *J. Org. Chem.* **2011**, *76*, 450–459.

[12] B. D. Fairbanks, E. V. Sims, K. S. Anseth, C. N. Bowman, *Macromolecules* **2010**, *43*, 4113–4119.

[13] a) B. Jacobsen, M. Ploug, *Curr. Med. Chem.* **2008**, *15*, 2559–2573.

[14] a) M. Persson, J. Madsen, S. Ostergaard, M. M. Jensen, J. T. Jogensen, K. Juhl, C. Lehmann, M. Ploug, A. Kjaer, *J. Nucl. Med.* **2012**, *53*, 138–145; b) M. Persson, H. Liu, J. Madsen, Z. Cheng, A. Kjaer, *Nucl. Med. Biol.* **2013**, *40*, 618–624.

[15] R. van Geel, G. J. M. Pruijn, F. L. V. Delft, W. C. Boelens, *Bioconjugate Chem.* **2012**, *23*, 392–398.

[16] Z. B. Li, G. Niu, H. Wang, *Clin. Cancer Res.* **2008**, *14*, 4758–4766.

Received: February 3, 2015
Published online: March 20, 2015

